Contrib Mineral Petrol (2006) 152:243–256
DOI 10.1007/s00410-006-0107-2

ORIGINAL PAPER

# Dynamic melting of the Precambrian mantle: evidence from rare earth elements of the amphibolites from the Nellore–Khammam Schist Belt, South India

**K. Vijaya Kumar · M. Narsimha Reddy · C. Leelanandam**

Received: 2 March 2005 / Accepted: 25 April 2006 / Published online: 14 June 2006


**Abstract** The Nellore–Khammam Schist Belt (NKSB) in South India is a Precambrian greenstone belt sited between the Eastern Ghats Mobile Belt (EGMB) to the east and the Cratonic region to the west. The belt contains amphibolites, granite gneisses and metasediments including banded iron formations. Amphibolites occurring as dykes, sills and lenses—in and around an Archaean layered complex—form the focus of the present study. The amphibolites are tholeiitic in composition and are compositionally similar to Fe-rich mafic rocks of greenstone belts elsewhere. The NKSB tholeiites show highly variable incompatible trace element abundances for similar Mg#s, relatively constant compatible element concentrations, and uniform incompatible element ratios. Chondrite-normalized REE patterns of the tholeiites range from strongly LREE depleted ($(La/Yb)_N = 0.19$) to LREE enriched ($(La/Yb)_N = 6.95$). Constant $(La/Ce)_N$ ratios but variable $(La/Yb)_N$ values are characteristic geochemical traits of the tholeiites; the latter has resulted in crossing REE patterns especially at the HREE segment. Even for the most LREE depleted samples, the $(La/Ce)_N$ ratios are > 1 and are similar to those of the LREE enriched samples. There is a systematic decrease in $FeO^t$, $K_2O$ and $P_2O_5$, as well as Ce and other incompatible elements from the LREE enriched to the depleted samples without any variation in the incompatible element ratios and Mg#s. Neither batch and fractional melting, nor magma chamber processes can account for the non-correlation between the LREE enrichment and HREE concentrations. We suggest that dynamic melting of the upper mantle is responsible for these geochemical peculiarities of the NKSB tholeiites. Polybaric dynamic melting within a single mantle column with variable mineralogy is the likely mechanism for the derivation of NKSB tholeiitic melts. It is possible that the NKSB tholeiites are derived from a source with higher FeO/MgO than that of present day ridge basalts.

**Keywords** Amphibolite · Nellore–Khammam schist belt · India · Rare earths · Geochemistry · Dynamic melting

Communicated by I. Parsons

K. Vijaya Kumar (✉)
School of Earth Sciences,
Swami Ramanand Teerth Marathwada University,
Nanded 431 606, Maharashtra, India
e-mail: vijay_kumar92@hotmail.com

M. Narsimha Reddy · C. Leelanandam
Department of Geology, Osmania University,
Hyderabad 500 007, Andhra Pradesh, India

## Introduction

Langmuir et al. (1977) introduced the dynamic melting model to explain the compositional variations in ocean-floor basalts from the FAMOUS area in the north Atlantic. The basalts, possibly derived from a single homogeneous source, show unusual trace element characteristics including crossing REE patterns but with constant incompatible element ratios for similar high Mg#s. Langmuir et al. (1977) suggested that these characteristics were the result of different degrees of both batch melting and continuous melting. Continuous melting can be defined as an intermediate process between batch and fractional melting, where

the instantaneous melt is continuously but not completely removed, so a part of the melt is always retained in the residue. A review of the mathematical equations for dynamic melting models is provided by Shaw (2000).

The dynamic melting model has been successfully used to explain the trace element systematics of basaltic and related rocks from a variety of geodynamic settings including tholeiites from the Mid-Atlantic ridge, Iceland, Troodos massif, Hawaii and Newfoundland, and cogenetic komatiites and basalts from Gorgana (Langmuir et al. 1977; Wood 1979; Strong and Dostal 1980; Elliott et al. 1991; Eggins 1992; Sobolev and Shimizu 1993; Gurenko and Chaussidon 1995; Arndt et al. 1997a). The applicability of dynamic melting is further broadened by Zou and Zindler (1996) through their dynamic melting inversion model, based on the method of Maaløe (1994), which calculates the source composition and the percentage of partial melting for cogenetic primary mantle-derived melts using the concentration ratios in magmas.

All of the above mentioned examples are from Phanerozoic associations from known tectonic environments, excepting the Newfoundland tholeiites, which are Neoproterozoic in age. In the present paper we show that the dynamic melting model can also explain the compositional variation within the tholeiites from a Palaeoproterozoic greenstone belt in South India. We utilize rare earth element concentrations of the rocks to model the melting processes as it has been shown that REE are more sensitive to dynamic (continuous) melting of the mantle (Langmuir et al. 1977; Hanson and Langmuir 1978; Langmuir and Hanson 1980). The importance of the NKSB dynamic partial melts is twofold. First, their composition suggests that melt generation processes similar to those operating in present day ocean basins operated at least as far back as the Palaeoproterozoic. Second, as the dynamic melts represent instantaneous melt compositions derived from the mantle, contrasts in the composition of the NKSB and the present day basalts can be used to understand the temporal evolution of the upper mantle composition and/or conditions of melting.

## Geological setting and petrography

The curvilinear Nellore–Khammam Schist Belt (NKSB) in South India (Fig. 1) is ~600 km long and between 30 and 130 km wide. The NKSB is sandwiched between the granulitic rocks of the Eastern Ghats Mobile Belt (EGMB) to the east and the Cratonic region to the west. The belt contains amphibolites, granite gneisses and metasediments including banded iron formations. Similar lithological associations elsewhere have been attributed to a shallow-marine platform setting (Arndt et al. 1997b). Although, certain segments of the belt are considered to be similar to Sargur-type ''Archaean'' greenstone belts of the Dharwar craton (Naqvi and Rogers 1987; Babu 1998), recent workers have assigned a Palaeo- to Meso-Proterozoic age to the NKSB (see Ramakrishnan 2003). The only reliable age data come from $^{207}Pb$-$^{206}Pb$ single grain evaporation ages for magmatic zircons from metarhyolites (1868 ± 6 and 1771 ± 8 Ma; Vasudevan et al. 2003). Some of the xenocrystic zircons in these possible crustal melts yield ages up to 2,431 Ma (Vasudevan et al. 2003), suggesting that the belt is at least Palaeoproterozoic in age. Based on limited geochemical studies on the metavolcanic rocks, earlier workers have proposed marginal basin, back-arc, oceanic island arc and continental margin arc tectonic settings for the NKSB (Satyanarayana et al. 1994; Hari Prasad et al. 2000). The rocks of the NKSB have undergone polyphase deformation and show a prominent NNE–SSW to NE–SW fabric in the northern parts (Sarvothaman 1995). There is a general increase in the grade of metamorphism from west to east. The mafic rocks are mainly of basaltic composition and occur as dykes, sills, lenses and flows. They have undergone amphibolite grade metamorphism, although local granulite grade rocks are not uncommon. Rocks of komatiite composition are yet to be reported from the NKSB. The present study area is in the NE part of the NKSB (shown in box in Fig. 1), where the Chimalpahad intrusion—the largest Archaean-type layered anorthosite complex in Peninsular India—is located (Leelanandam and Narsimha Reddy 1985; Ashwal 1993). The samples for the present study were collected from dykes, sills and lenses in and around the Chimalpahad layered complex (Fig. 1). Field relations suggest that all the dykes and sills were emplaced in a single episode. Understanding the origin of the tholeiites is vital in evaluating the geodynamic setting for the NKSB and to unfold the proposed collision tectonics between the Eastern Ghats Mobile Belt and Dharwar Craton (Radhakrishna and Naqvi 1986).

Although amphibolite to granulite grade metamorphism has altered the original textures and mineralogy of the mafic rocks, many of the samples in our collection show relict igneous textures and clinopyroxenes. Textures displayed by the amphibolites include fine grained aphanitic, intergranular, medium to coarse grained equigranular, granuloblastic (those which are highly deformed) and granulose (those with clinopyroxene >> hornblende). In rare cases, some of the

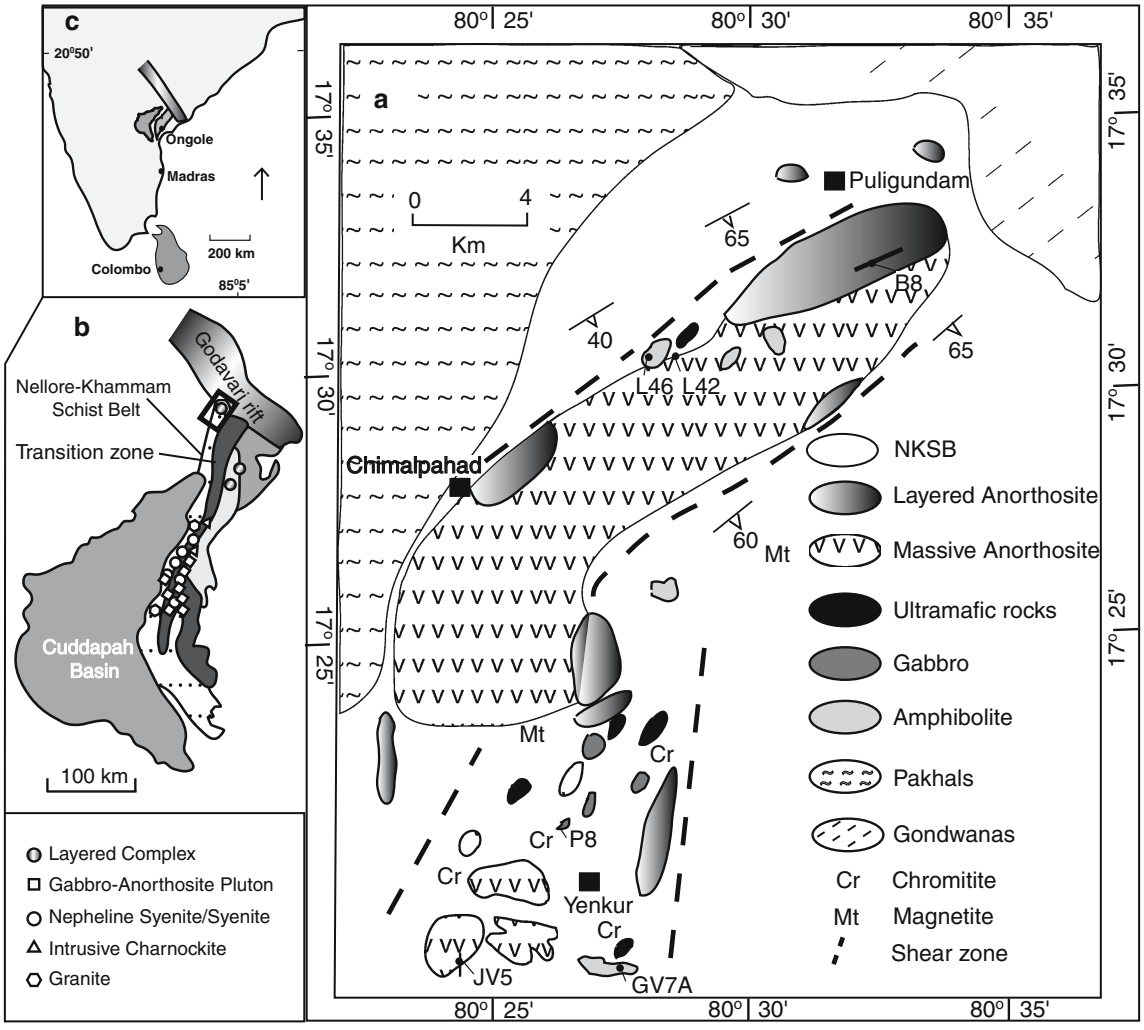


**Fig. 1** **a** Geological map of a part of the Nellore–Khammam Schist Belt (NKSB; modified after Appavadhanulu et al. 1976) marked with sample locations. Pakhals are Proterozoic sedimentary formation and Gondwanas are upper Permian to lower Cretaceous sedimentary supergroup. The inset maps (**b**, **c**) show the location of the NKSB within the Peninsular India

high MgO rocks show skeletal amphiboles (originally pyroxenes) suggesting a possible spinifex texture. The essential mineralogy of the amphibolites is simply plagioclase + amphibole, but their relative proportions are highly variable. Quartz, garnet, epidote, sphene, clinopyroxene, and magnetite/ilmenite are the subordinate minerals, though all of them do not occur in a single rock. Mafic rocks which have attained granulite grade metamorphism contain higher modal pyroxene than amphibole.

## Geochemical characteristics of the amphibolites

Major and trace element compositions of the representative amphibolites from the study area are given in Table 1. The amphibolites have restricted range of $SiO_2$ (46.16–50.93 wt%; anhydrous basis) and low $Al_2O_3$ (11.89–15.51); they contain high contents of $FeO^t$ ($Fe_2O_3^t$ = 12.72–15.54 wt%) which lead to relatively lower Mg#s. Mg#s of the amphibolites have an extended range from 0.65 to 0.38, and the normative anorthite content varies from 0.72 to 0.44. $TiO_2$ varies by a factor of two (from 0.35 to 0.83 wt%) for samples with similar Mg#s, but the more fractionated samples (lower Mg#s and higher REE) contain $TiO_2$ up to 1.65 wt%. CaO varies from 10.19 to 13.82 wt% and the rock (JV5) with highest CaO content contains lowest REE abundances. None of the samples are cumulates as indicated by the trace element abundances. Normatively, the amphibolites are quartz and olivine tholeiites; only two samples (JV5 and P8) show nepheline in the norm. We retain the term 'tholeiite' for the NKSB amphibolites in the following discussion.

**Table 1** Representative major and trace element composition of the NKSB tholeiites

| | JV5 | B8 | GV7A | L42 | L46 | P8 |
|---|---|---|---|---|---|---|
| Major elements normalized to 100 wt% on an anhydrous basis | | | | | | |
| $SiO_2$ | 46.16 | 49.83 | 50.63 | 47.66 | 50.93 | 47.82 |
| $TiO_2$ | 0.35 | 0.43 | 0.47 | 0.90 | 0.49 | 0.83 |
| $Al_2O_3$ | 14.11 | 11.89 | 13.08 | 14.37 | 15.51 | 11.98 |
| $Fe_2O_3^a$ | 12.85 | 14.71 | 13.62 | 14.57 | 12.72 | 15.54 |
| MnO | 0.20 | 0.27 | 0.21 | 0.20 | 0.04 | 0.23 |
| MgO | 10.38 | 8.76 | 8.93 | 7.95 | 7.46 | 9.77 |
| CaO | 13.82 | 12.29 | 11.24 | 11.70 | 10.28 | 10.19 |
| $Na_2O$ | 2.03 | 1.59 | 1.73 | 2.14 | 1.85 | 3.04 |
| $K_2O$ | 0.06 | 0.19 | 0.08 | 0.40 | 0.58 | 0.50 |
| $P_2O_5$ | 0.03 | 0.03 | 0.01 | 0.10 | 0.14 | 0.10 |
| Total | 99.29 | 99.04 | 98.53 | 97.75 | 102.51 | 97.16 |
| $Mg/(Mg + Fe^{total})$ | 0.61 | 0.54 | 0.56 | 0.52 | 0.54 | 0.55 |
| $Mg/(Mg + Fe^{2+})$ | 0.65 | 0.58 | 0.60 | 0.56 | 0.58 | 0.59 |
| An/An+Ab | 0.72 | 0.65 | 0.65 | 0.61 | 0.67 | 0.43 |
| Trace elements in ppm | | | | | | |
| Ni | 499.3 | 289.8 | 149 | 164 | 220 | 350.6 |
| Cr | 725.5 | 444 | 114.9 | 316.4 | 542.9 | 1018.7 |
| Co | 84.5 | 102.1 | 57.4 | 67 | 69.9 | 83.4 |
| V | 105.2 | 417.1 | 254.9 | 445.7 | 500.5 | 327.2 |
| Sc | 68.2 | 72.8 | 50.9 | 53.2 | 56.3 | 32.3 |
| Rb | 3 | 2.7 | 8.8 | 14.6 | 15.3 | 5 |
| Sr | 92.8 | 35.6 | 133.2 | 97.9 | 115.5 | 147.6 |
| Ba | 19 | 38 | 57.5 | 118.9 | 141.3 | 326.7 |
| Y | 18.35 | 17.7 | 18.82 | 21.7 | 17.44 | 22.9 |
| Zr | 5.3 | 5.16 | 10.62 | 19.3 | 17.78 | 103.7 |
| Nb | 0.39 | 0.11 | 5.56 | 3.93 | 2.46 | 6.5 |
| Hf | 0.46 | 0.14 | 0.56 | 0.53 | 0.6 | 2.25 |
| Ta | 0.04 | 0.25 | 0.39 | 0.52 | 0.15 | 0.33 |
| Th | 0.12 | ND | 0.93 | 0.87 | 0.72 | 1.79 |
| U | 0.05 | ND | 0.61 | 0.19 | 0.17 | 3.69 |
| Rare earth elements in ppm | | | | | | |
| La | 0.36 | 0.74 | 1.9 | 4.98 | 6.25 | 19.59 |
| Ce | 0.85 | 1.56 | 4.58 | 12.41 | 12.46 | 42.25 |
| Nd | 0.81 | 1.24 | 3.34 | 6.4 | 5.58 | 16.08 |
| Sm | 0.44 | 0.51 | 1.34 | 2.04 | 2.02 | 3.6 |
| Eu | 0.15 | 0.23 | 0.43 | 0.83 | 0.48 | 0.91 |
| Gd | 0.8 | 1.1 | 2.3 | 2.6 | 2.21 | 3.62 |
| Tb | 0.17 | 0.25 | 0.38 | 0.46 | 0.35 | 0.6 |
| Yb | 1.28 | 1.52 | 2.4 | 1.75 | 1.55 | 1.86 |
| Lu | 0.2 | 0.31 | 0.34 | 0.28 | 0.26 | 0.29 |
| Total REE | 5.06 | 7.46 | 17.01 | 31.75 | 31.16 | 88.8 |

Major elements (in wt%) and trace elements (in ppm) are on anhydrous basis. Major elements by XRF; trace and REE on ICP-MS

*ND* Not determined

[a] Total Fe as $Fe_2O_3$; $Fe^{2+}/Fe^{tot}$ is taken as 0.85

Chondrite-normalized REE patterns of the tholeiites (Fig. 2), covering the entire compositional spectrum range from strong relative LREE depletion ($(La/Yb)_N = 0.19$) to LREE enrichment ($(La/Yb)_N = 6.95$) with small negative Eu anomalies. $(Sm/Yb)_N$ ratios (0.36–2.10) in the NKSB tholeiites show the widest range found in any single suite of comparable rocks from anywhere in the world. Eu anomalies in these rocks are attributed to alteration. The samples which show LREE enriched patterns contain relatively lower $Al_2O_3/TiO_2$ and $CaO/TiO_2$ values than the samples with the LREE depleted patterns. Constant $(La/Ce)_N$ ratios but variable $(La/Yb)_N$ values (Table 2) are characteristic geochemical traits of the tholeiites; the latter has resulted in crossing REE patterns, especially at the HREE end of the normalized REE profiles. Even for the most LREE depleted samples (JV5 and B8), the $(La/Ce)_N$ ratios are > 1 and are similar to the LREE enriched ones (L42 and P8). The LREE enrichment does not correlate with the HREE abundances, as in the case with the FAMOUS glasses (Langmuir et al. 1977).

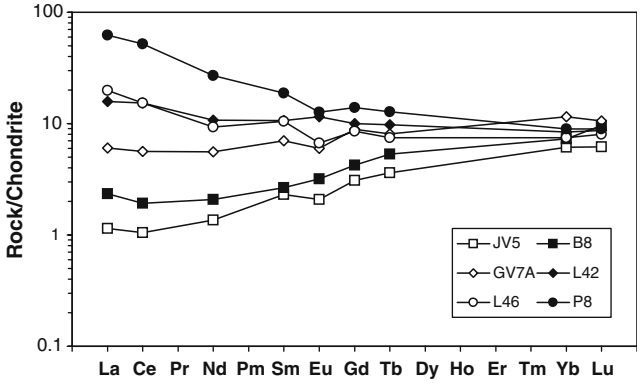


**Fig. 2** Chondrite-normalized REE patterns for the NKSB tholeiites. Normalizing values (after Masuda et al. 1973) are as reported in Hanson (1980). The petrogenetic discussion is based on these REE patterns smoothed by removal of Eu

Some of the LREE depleted REE patterns for the NKSB tholeiites are as low as any reported for rocks of basaltic composition from the Precambrian greenstone belts (Sun and Nesbitt 1978; Kerrich et al. 1998), and are comparable to LREE depleted modern ocean floor basalts and glass inclusions (Frey et al. 1974; Kay et al. 1970; Sobolev and Shimizu 1992, 1993). We have used the least differentiated samples (MgO > 7.5 wt%) for evaluating the partial melting processes.

Chemical mobility of elements is a common problem associated with alteration and amphibolite-granulite grade metamorphism of rocks of basaltic composition (Sun and Nesbitt 1978; Thompson 1991). Therefore, it is mandatory to assess the relative mobility of the elements before subjecting the elemental abundances to petrogenetic interpretations. We have used Zr as a monitor to assess the mobility of the elements, since it is considered that Zr is immune to chemical mobility under most metamorphic conditions and alteration (Pearce and Cann 1973; Weaver and Tarney 1981; Sheraton 1984). Mantle melting and basaltic magma crystallization do not change the ratios of very incompatible elements; as a result, the incompatible elements are expected to show systematic covariance with Zr. Most studies have shown that the large ion lithophile elements (Rb, Ba, Sr, K, Na etc.) are relatively mobile, whereas the high field strength elements (Zr, Hf, Nb, Ta, Y, REE etc.) show little or no mobility. Our data reflect variable migration of elements in the NKSB tholeiites (Fig. 3). La and Ce show very good correlations against Zr with correlation coefficients > 0.9 (Fig. 3a, b). Although some examples of La mobility in basalts have been reported (for example Frey et al. 1974), La appears to behave consistently along with the other rare earth elements in the NKSB tholeiites (Figs. 2, 3a; Table 2) suggesting that La concentrations reflect original igneous abundances. Additionally, the rocks JV5 and P8 with lowest (5.06 ppm) and highest (88.8 ppm) REE concentrations respectively are both olivine normative, suggesting that the variable REE patterns are their original traits and have not been modified by metamorphism and alteration. However, the Eu abundances seem to be modified by alteration as the samples show both positive and negative anomalies, which do not correlate with their $Al_2O_3$ abundances. Elements that typically are more mobile, such as Rb (Fig. 3c) show only limited mobility (especially in the samples with higher abundances), but Ba (Fig. 3d), K (Fig. 3e) and Sr (Fig. 3f) appear to be more mobile. One should be cautious when interpreting this co-linearity because it applies only to the highly incompatible elements; elements such as Y, Nb, Yb etc. *do not* show linear trends against Zr, if their abundance distribution is controlled by polybaric melting of the mantle. In such a case Zr/Y and Zr/Nb ratios show a wide range (see Table 2). Our petrogenetic interpretations are based on the REE, which seem to be least mobile in the NKSB basaltic rocks, and thus record original igneous compositions. The petrogenetic discussion is based on REE patterns smoothed by the removal of Eu.

## Evidence for dynamic melting

First, we evaluate the primitive nature of the NKSB tholeiites, since they show lower Mg#s than mantle-derived primary basaltic magmas and subsequently test the hypothesis of dynamic melting of mantle for their origin. We utilize the [Mg]–[Fe] model of Rajamani et al. (1993) to assess the source characteristics in terms of Mg and Fe. [Mg] and [Fe] (Fig. 4a) are compositionally corrected Mg and Fe abundances in cation mole percent using Eq. 3 of Ford et al. (1983) for the compositionally corrected olivine-melt distribution coefficients ($K_D$ values) for MgO and FeO. Melt fields for Gt lherzolite mantle at 0, 3 and 5 G Pa pressures are shown in Fig. 4a. The size of the melt field decreases with increasing pressure. The NKSB tholeiites and FAMOUS basalts are plotted in the [Mg]–[Fe] diagram (Fig. 4a). Representative REE patterns for both the NKSB tholeiites and FAMOUS basalts are shown in Fig. 4b and c, respectively. The melts formed by continuous melting of the mantle exhibit a trend towards lower [Fe] and higher [Mg] values ''because the bulk composition of the effective parent moves to lower FeO and higher MgO abundances as the melting proceeds'' (Hanson and Langmuir 1978). This [Fe] depletion is correlatable with a remarkable decrease in

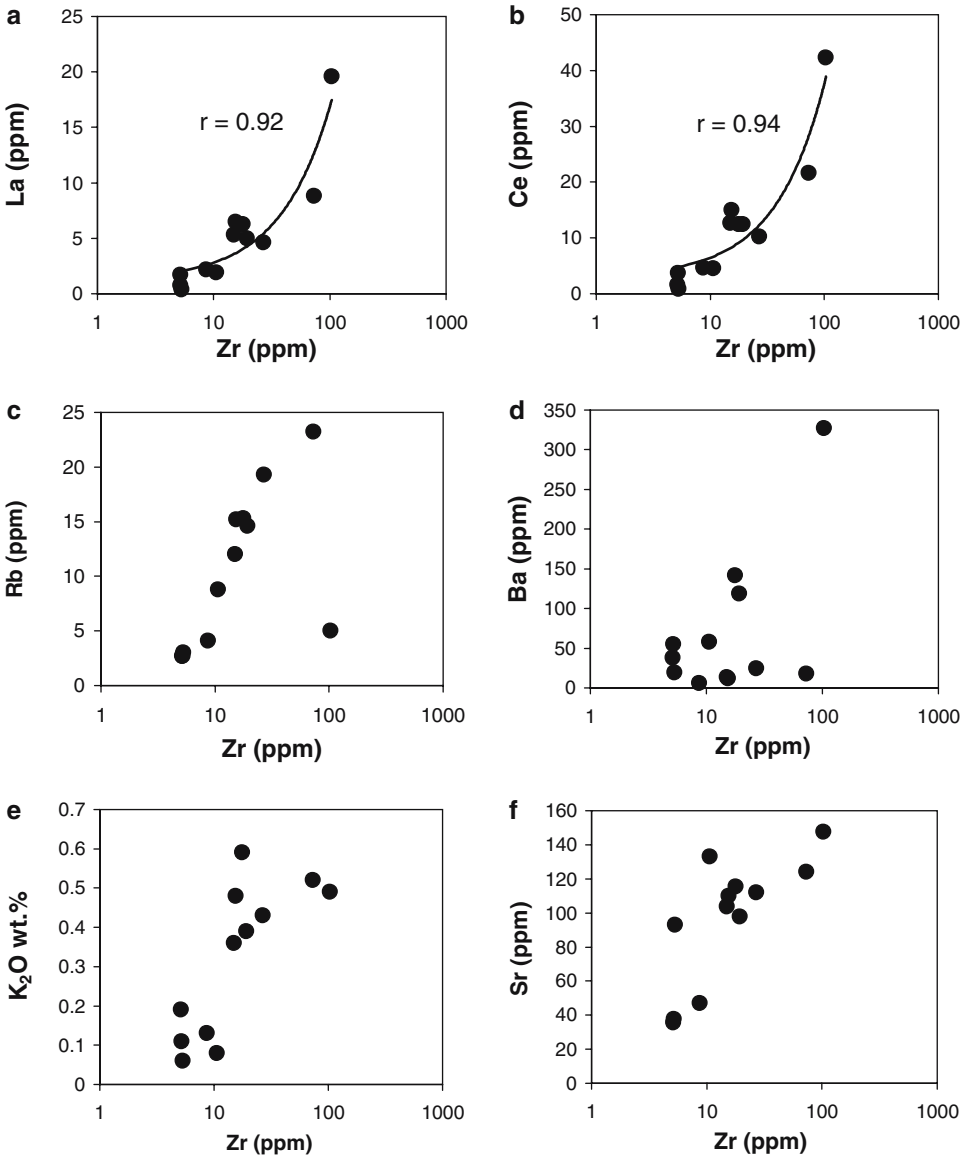


**Fig. 3** Zr vs incompatible element variation in all the analyzed NKSB tholeiites. Strong positive correlation for La and Ce suggests little mobility of REE due to metamorphism in the NKSB tholeiites. For discussion see the text

**Table 2** Petrogenetic parameters for the samples shown in Fig. 2

| Sample No. | Mineralogy | Mg # | La | Nature of REE pattern | $(La/Yb)_N$ | $(La/Ce)_N$ | Ce/Zr | (Ti/Y)/100 | Zr/Y |
|---|---|---|---|---|---|---|---|---|---|
| *JV5* | (Hbl + Pl + Gt (tr)) | 0.61 | 0.36 | LREE depleted | 0.19 | 1.09 | 0.16 | 1.14 | 0.29 |
| *B8* | (Pl + Hbl + Cpx) | 0.54 | 0.74 | LREE depleted | 0.32 | 1.22 | 0.30 | 1.45 | 0.29 |
| *GV7A* | (Hbl + Pl + Epi) | 0.56 | 1.90 | LREE depleted | 0.52 | 1.07 | 0.43 | 1.46 | 0.56 |
| L42 | (Pl + Cpx + Hbl + Gt + Opx) | 0.52 | 4.98 | LREE enriched | 1.88 | 1.04 | 0.64 | 2.43 | 0.89 |
| *L46* | (Hbl + Pl + Scp + Epi) | 0.54 | 6.25 | LREE enriched | 2.66 | 1.29 | 0.70 | 1.71 | 1.02 |
| P8 | (Pl + Cpx + Hbl + Opx + Gt) | 0.55 | 19.59 | LREE enriched | 6.95 | 1.20 | 0.41 | 2.12 | 4.53 |

*Hbl* Hornblende, *Pl* Plagioclase, *Gt* Garnet, *Cpx* Clinopyroxene, *Epi* Epidote, *Opx* Orthopyroxene, *Scp* Scapolite

Mg # = $Mg/(Mg + Fe^{total})$

rare earth element abundances especially in the LREE (Fig. 4b, c). During continuous melting, melts with higher [Fe] values and REE abundances (with enriched LREE patterns) represent the first increments derived from the ''fertile'' source, and melts with lower [Fe] and REE concentrations (with ultra-depleted LREE patterns), and slightly higher Mg#s and compatible element concentrations,

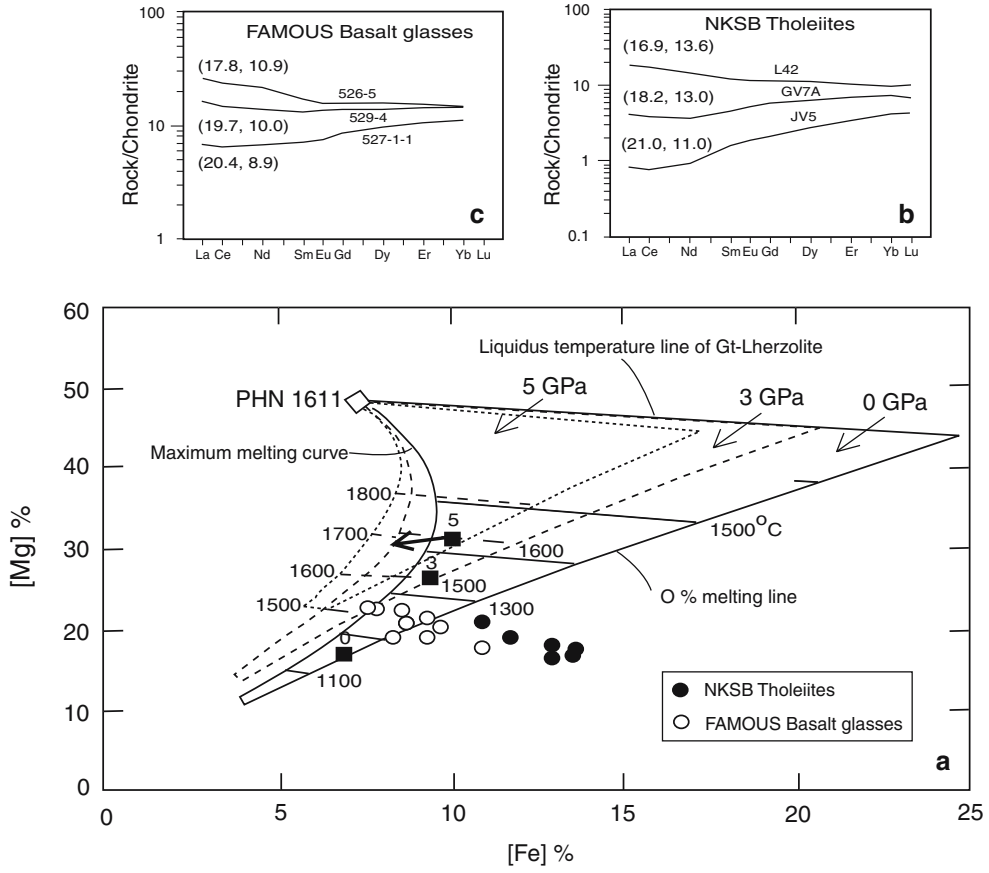


**Fig. 4** **a** [Fe]–[Mg] diagram (after Rajamani et al. 1993) for the primitive NKSB tholeiites, showing melt fields for batch melting of Gt lherzolite (PHN 1611; open rhomb) at 0, 3 and 5 GPa. The melt field shrinks as pressure increases and is bounded on the right by 0% melting line where the incipient melt formed is in equilibrium with all the mantle phases. The maximum extent of melting at a given temperature is shown by left boundary curve (maximum melting curve) where the melt is in equilibrium only with olivine. The upper boundary line of the melt field is the liquidus temperature of the mantle, which varies with pressure. The solidii for 0, 3 and 5 GPa pressures (*solid squares*) are based on the experimental work of Takahashi (1986). A possible path of adiabatic melting is given by the *thick arrow*. During continuous melting of the mantle the melting path moves towards lower [Fe] and higher [Mg] values because the bulk composition of the effective parent moves to lower FeO and higher MgO abundances as the melting proceeds (Hanson and Langmuir 1978). Basalts from the FAMOUS area (Langmuir et al. 1977) are also plotted. **b** Representative REE patterns of the NKSB tholeiites. Sample P8 and other fractionated samples have been omitted. **c** Representative REE patterns for Famous basalts. Sample numbers and ([Mg], [Fe]) values are shown on the curves in **b** and **c**

represent the last increments derived from 'refractory' source that has already undergone melt extraction. In a way, the systematic changes in a cogenetic suite of rocks formed by continuous melting are reverse of what one might expect from differentiation through fractional crystallization of a single parental magma. In spite of their extreme depletion in LREE, the melts formed by continuous melting show constant La/Ce values (Fig. 4b, c). This is due to the fact that during continuous melting, a small melt fraction is retained with the residue (effective parent). This small melt fraction enables the residue to retain the constant La/Ce ratio, though the overall REE pattern progressively shifts to LREE depletion as the melting proceeds. Both the NKSB tholeiites and the FAMOUS basalts strikingly display this characteristic feature (Fig. 4b, c).

The trends of the NKSB tholeiites and FAMOUS basalts are similar in the [Mg]–[Fe] diagram but the former have at least 2% higher [Fe] values than the latter for comparable [Mg] values. Three possible reasons for higher [Fe] abundances in the NKSB tholeiites could be: (1) extensive fractional crystallization of clinopyroxene (± olivine), (2) derivation from sources that have greater FeO/MgO ratios than the present day MORB mantle or (3) melting at greater pressures (depths).

Fractional crystallization involving olivine and clinopyroxene results in wide variation in Mg#s and compatible element concentrations whereas different degrees of melting of mantle under similar conditions

would result in melts with a limited range in Mg#s and compatible element abundances (Rajamani et al. 1989) as characteristically shown by the NKSB tholeiites. Even if clinopyroxene fractionation is assumed, it requires at least 25% of clinopyroxene removal to account for change in the [Fe] values (from 11 to 13.6; Fig. 4) and Cr concentrations (from 725 to 315 ppm; Table 1) for samples JV5 and L42. For 25% clinopyroxene removal from JV5, La increases from 0.36 to 0.50 ppm, where as La in L42 is 4.98 ppm. The possibility of clinopyroxene fractionation is further negated by high CaO contents in the NKSB tholeiites comparable to the most primitive basalts from FAMOUS and elsewhere. It is much more difficult to explain the huge range in REE abundances for a limited variation in Mg#s (Table 1) with olivine fractionation, which has very high $K_d$ for Mg and insignificant partition coefficients for REE. Further, extensive fractional crystallization of mafic phases is unlikely due to higher abundances of Ni and Cr in the NKSB tholeiites. Therefore, based on the above arguments, we suggest that the higher [Fe] values and variable REE abundances in the NKSB tholeiites have an origin in the mantle.

Systematic compositional variations, especially in the [Fe] contents of Palaeoproterozoic NKSB tholeiites and present day ridge basalts strongly suggest either that the depth of melting of the upper mantle has decreased with time or that the mantle sources for NKSB tholeiites are Fe-rich than the present day MORB sources. The indistinguishable [Mg] contents of NKSB tholeiites and FAMOUS basalts rules out any significantly higher potential temperature, consequently pressures, for the NKSB mantle. Further, parental melts to the Palaeoproterozoic NKSB tholeiites (present study), Neoproterozoic Newfoundland tholeiites (Strong and Dostal 1980) and the modern FAMOUS basalts (Langmuir et al. 1977) all are possibly derived within the garnet-spinel and spinel stability fields, suggesting similar depths of derivation. Based on the above arguments, we infer that the lower Mg#s in the NKSB tholeiites, giving an apparent evolved character to the rocks, in fact are a reflection of an Fe-rich mantle source. The present study supports the proposed existence of Fe-rich mantle sources during the Archaean and Palaeoproterozoic as exemplified by Francis et al. (1999) and Hanski and Smolkin (1995). We suggest that the compositional variations in the NKSB tholeiites are controlled by source composition, depth, degree and type of melting, with fractional crystallization and crustal contamination having little influence.

Relevant petrogenetic parameters of the tholeiites are given in Table 2. Characteristic features of the NKSB tholeiites are the constant incompatible element ratios for similar Mg#s, and highly variable La concentrations and REE slopes as demonstrated by $(La/Yb)_N$ ratios (Table 2). Fractional crystallization, batch melting and fractional fusion, are not capable of producing the entire range of concentrations displayed by the NKSB tholeiites. Fractional crystallization can not change the $(La/Yb)_N$ ratio from 0.19 to 6.95 and La concentrations from 0.36 to 19.59 ppm (Table 1) without significantly affecting the Mg# and compatible element concentrations, for any set of minerals fractionating in a basaltic magma. Our samples show similar Mg#s and similarly high compatible element concentrations. Further, batch melting and fractional melting of a homogeneous source are not capable of producing crossing REE patterns.

Figure 5 shows melt compositions for different extents of batch, fractional and continuous melting of a mantle source with $La_N = 3.6$ and $(La/Sm)_N = 2.57$. Details of the calculation of the source composition are given in the caption to Fig. 6. It is evident that the compositional variations in the NKSB tholeiites are best explained by continuous melting of the source. Melts formed by batch and fractional melting show higher and lower abundances respectively, than the observed concentrations. Some of the REE compositions could be explained by batch or fractional melting of the mantle source but neither model can produce the entire range of REE compositions displayed by the NKSB tholeiites. Although fractional melt compositions merge with the observed $La_N$ and $(La/Sm)_N$ values, especially in the rocks with higher $La_N$ values, fractional melting is not capable of delivering the constant $(La/Ce)_N$ ratios observed in the NKSB tholeiites; fractional melting depletes La over Ce as the melting proceeds, and hence melts show progressive decrease in La/Ce ratios rather than constant values. Langmuir et al. (1977) have suggested that LREE enriched and depleted patterns, crossing of REE patterns and reasonably constant La/Ce ratios are characteristics of melts produced by dynamic (continuous + batch) melting processes. The NKSB tholeiites show all these features (Table 2) and so in the section below, we test the hypothesis that the tholeiites were produced by dynamic melting of a homogeneous source.

In the modeling calculations, it is surmised that melting begins in the Gt–Sp lherzolite stability field; as melting progresses, the rising mantle column passes in sequence through Sp lherzolite, Sp–Pl lherzolite and Pl lherzolite, a similar progression to that proposed by Prinzhofer and Allegre (1985), McKenzie and O' Nions (1991) and Gurenko and Chaussidon (1995). Melting events producing both the LREE enriched and

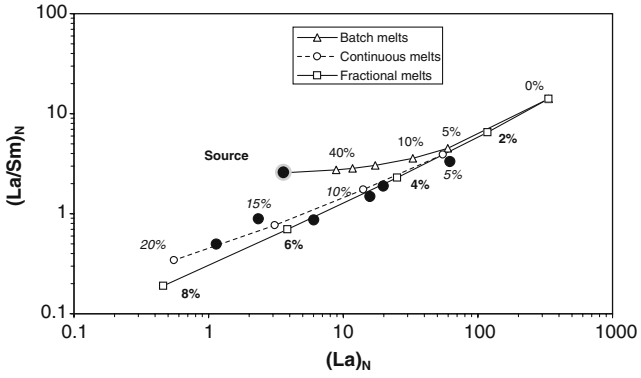


**Fig. 5** $La_N$ versus $(La/Sm)_N$ variation in the NKSB tholeiites. Curves for batch, fractional and continuous melting have been calculated for different extents of melting of a source with $La_N = 3.6$ and $(La/Sm)_N = 2.57$. Melting equations are given in Appendix. The NKSB tholeiites plot along the continuous melting curve of the mantle; batch and fractional melting compositions are higher and lower respectively than the observed concentrations. For fractional fusion, the source is melted by 2%, the melt produced is completely removed and the residue is melted further by 2% and so on; during continuous melting the melt produced is continuously but not completely removed with some percentage of melt constantly retained in the residue. Percentages of partial melting are indicated on the batch (in normal font), continuous (*italic*) and fractional (*bold*) melting curves

depleted patterns of the tholeiitic melts could have taken place within the rising mantle column progressively in the Gt–Sp lherzolite field and Sp lherzolite field. We see no samples which might have formed in the plagioclase stability field.

Figure 6 shows the calculated melt patterns for the mantle source for various extents of batch and continuous melting. Samples P8 and L46 might have been produced by 7 and 20% batch partial melting of a source of the composition shown in Fig. 6a. These melts are considered to have formed when the melting column was within the Gt–Sp lherzolite stability field. The composition of P8 which has the highest incompatible and transition element abundances, and an alkaline nature (nepheline in norm) suggests its derivation by low degree melting of a deeper source. It is well known that the transition element abundances (in a mantle derived melt) depend on the depth of melting, while the abundance of an incompatible element depends on the degree of melting (Langmuir and Hanson 1980; Rajamani et al. 1985). Samples L42, GV7A, B8 and JV5 have formed by continuous melting of the same source. Degrees of melting and the proportion of the melt retained within the residue are shown in Fig. 6b. During the derivation of the melts parental to samples L42, GV7A, B8 and JV5, it is assumed that the melting regime has entered the Sp lherzolite stability field. This assumption is based on the fact that the samples show flat to LREE depleted patterns, which requires exclusion of garnet in the source. Further, systematic decrease in Zr/Y ratio from P8 to JV5 with changing REE patterns from LREE-enriched to LREE-depleted (Table 2; Fig. 2) bears testimony to the changing physical conditions during melting (from Gt–Sp stability field to Sp stability field). We have used a critical (continuous) melting model (Sobolev and Shimizu 1992) for modeling melts formed by continuous melting. Mantle source mineralogy, melting proportions, and the mineral/melt partition coefficients are given in Appendix. A composite of the melts produced by both batch and continuous melting is shown in Fig. 6c and is compared to patterns for the NKSB tholeiites in Fig. 6d. Langmuir et al. (1977) considered such composite patterns to be a characteristic result of the dynamic melting process. Dynamic melting of the mantle explains the generation of melts with lower La (ultradepleted) than the source itself but without altering the La/Ce ratio of all the possible melts derived from a single homogeneous source.

## Discussion

In addition to the dynamic model presented here, source heterogeneity (Schilling 1973; Zindler et al. 1979) and magma chamber processes (Elthon 1984) are also capable of producing LREE enriched and depleted patterns for a cogenetic series of rocks. We appeal to constant incompatible element ratios in the NKSB tholeiites to argue against heterogeneous sources. Even if heterogeneous sources with similar incompatible element ratios are assumed, they can not produce the observed REE range of NKSB tholeiites by simple batch melting.

Lack of a correlation of LREE enrichment and HREE concentrations, high MgO, and high Ni abundances even in samples with low Mg#s can not be explained by magma mixing in a periodically replenished magma chamber. Further, for a 5% change in the Mg#, Sr and Zr vary by a factor of 5 and 20 respectively; this is difficult to reconcile even if a steady state (30–50 cycles) magma chamber is assumed. Therefore, we suggest that the trace element variation shown by the NKSB tholeiites is not an outcome of magma chamber processes but has an origin within the mantle. Although mixing may not produce the entire range of REE abundances in the NKSB tholeiites, it might have influenced the compositions of some. For example, sample B8 can be derived by mixing of samples JV5 and GV7A.

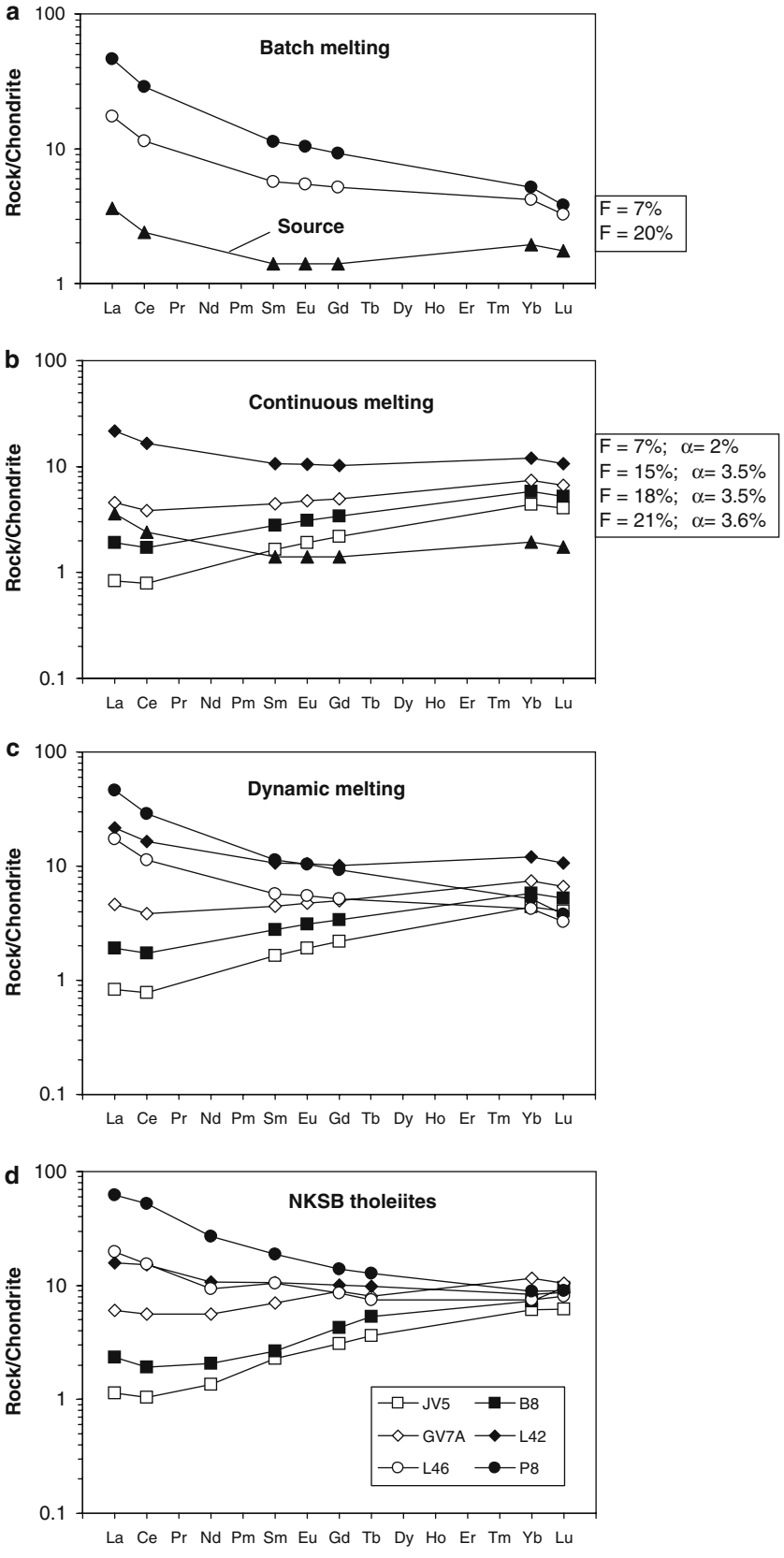


**Fig. 6** Proposed model for the generation of LREE enriched and depleted patterns from a homogenous source. Percentages of melting (F) and the melt fractions retained (α) are shown. **a** REE patterns produced by different extents of batch partial melting of a Gt–Sp lherzolite source. The source was calculated assuming that the sample P8 is derived by 6–8% of melting of the mantle source. The average composition thus produced is shown. **b** REE patterns derived by continuous melting of the same source in the Sp–lherzolite stability field. During continuous melting some percentage of melt is always retained in the residue. Samples L42, GV7A, B8 and JV5 were derived by 7, 15, 18 and 21% continuous melting of the mantle respectively. **c** Composite of **a** and **b** results in the dynamic melting model as suggested by Langmuir et al. (1977). **d** REE patterns smoothed by removal of Eu. Batch and continuous melting equations and the partition coefficients used in the calculations are given in Appendix

A cartoon summarizing the processes and products of dynamic melting of the NKSB mantle is shown in Fig. 7. The samples with enriched LREE patterns are derived from the Gt–Sp lherzolite stability field, and the samples with depleted LREE have a source in the Sp–lherzolite stability field. Average compositions of some elements for both LREE enriched and depleted samples are shown in Fig. 7. There is a continuous decrease in $FeO^t$, $K_2O$ and $P_2O_5$, as well as Ce and other incompatible elements from the former to the latter, which is expected from continuous melting of the mantle. Samples with enriched LREE and other incompatible elements (P8 and L46) are considered to be early derived melts whereas depleted melts (JV5 and B8) represent the final fractions of melts produced by critical (continuous) melting of the mantle. Irrespective of such a huge variation in the incompatible element concentrations, the Mg#s, Ce/Zr and $(La/Ce)_N$ ratios are constant for both the LREE enriched and depleted melts (Table 2). Average $FeO^t$ content of the enriched REE samples is 13.90 wt% and that of depleted samples is 12.21 wt% suggesting a marginal decrease in $FeO^t$ in the melts with progressive melting. Although the melts show a Fe-deficient trend with progressive dynamic melting, the absolute values are higher because melting of sources with higher FeO/MgO

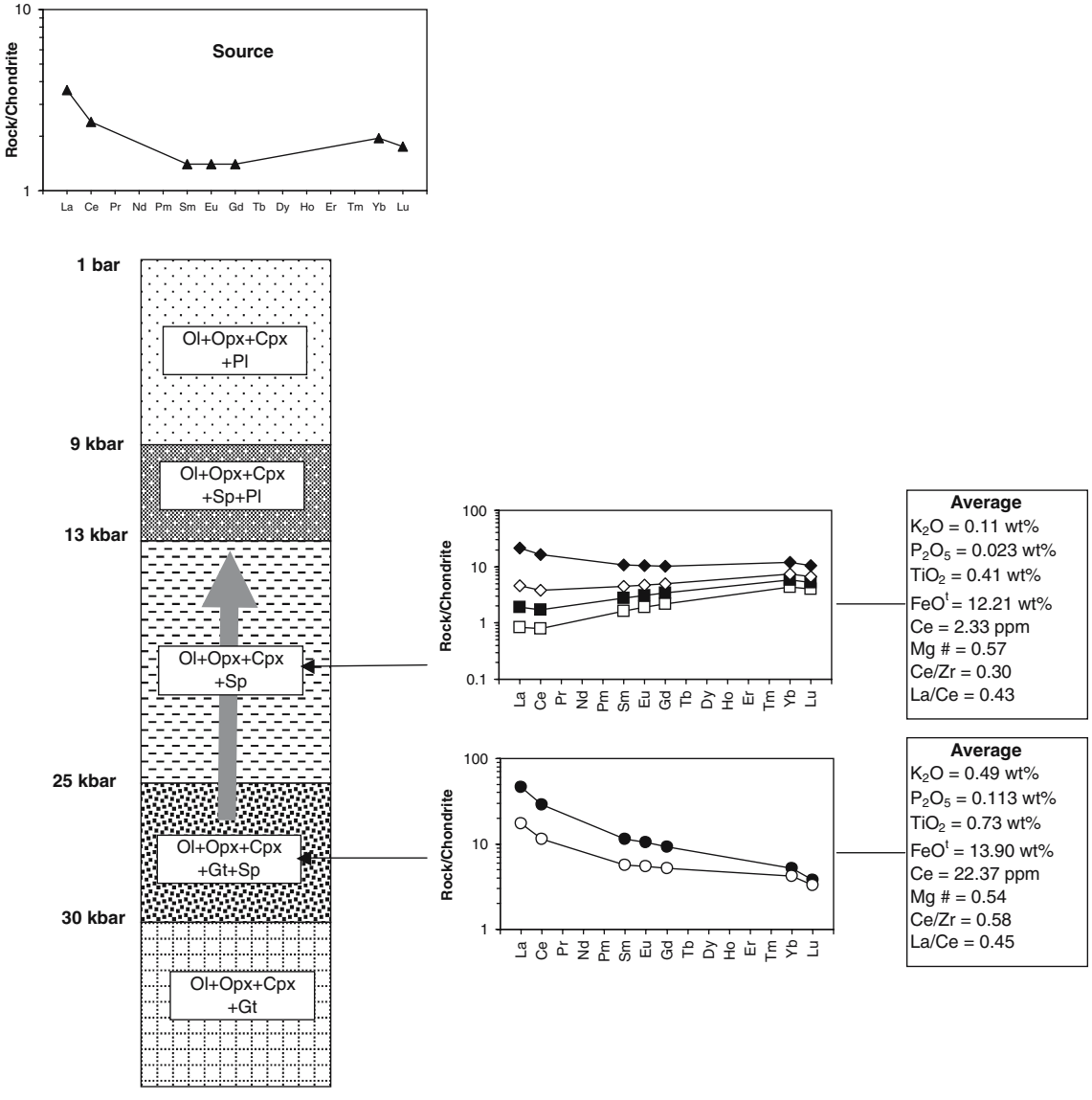


**Fig. 7** Cartoon illustrating the processes and products of dynamic melting. Average abundances of elements for LREE enriched and depleted groups are shown. Sample L42 was included in the enriched group. Boundaries for mantle phase assemblages are from Takahashi and Kushiro (1983) and Kinzler and Grove (1992)

ratios. Fe-enriched sources for the NKSB tholeiites is not at odds with general models for the origin of Archaean/Proterozoic mafic rocks (Rajamani et al. 1989; Hanski and Smolkin 1995; Francis et al. 1999). The proportional decrease of these elements is a function of the magnitude of their incompatibility with the mantle mineralogy. For instance, the proportional decrease in $FeO^t$ is 10%, while it is by a factor of 5 in $K_2O$ and $P_2O_5$ and a factor of 10 in Ce. The relative incompatibility of the elements during the dynamic melting of the NKSB mantle is in the order $Ce >> P_2O_5 \geq K_2O > FeO^t$. Available mineral/melt partition coefficient data do not negate the proposed order of incompatibility for a peridotitic mantle.

## Conclusions

The Precambrian tholeiites of the Nellore–Khammam Schist Belt of South India characteristically show variable incompatible trace element abundances for similar Mg#s, relatively constant transition element values and constant ratios for highly incompatible elements. The tholeiites show both LREE enriched and depleted patterns, but the LREE enrichment is not correlated with HREE abundances, leading to the crossing of REE patterns. This chemical divergence in the NKSB tholeiites has been evaluated using the dynamic melting model of Langmuir et al. (1977). The discovery of the products of dynamic partial melting in the Palaeoproterozoic NKSB when compared with the Neoproterozoic Newfoundland basalts (Strong and Dostal 1980) and modern ridge basalts (Langmuir et al. 1977) suggests no change in the processes of melt generation in the upper mantle through time, but it is possible that the NKSB tholeiites were derived from a source with higher FeO/MgO than that of the present day ridge basalts.

**Acknowledgments** We thank R. H. Smithies (Geological Survey of Western Australia) for a helpful review of an earlier version of the manuscript and Department of Science and Technology, Govt. of India, for funding (ESS/23/172/93). We also thank Ian Parsons for his skillful editorial handling.

## Appendix

Equations used in the calculations

1. Modal batch and fractional melting (Schilling 1966)

$$\frac{C_i^1}{C_i^0} = \frac{1}{[D_i^0(1-F)+F]} \quad (1)$$

(for fractional melting the residue is remelted after continuous and complete removal of 2% incremental melts)

2. Critical (continuous) melting (Sobolev and Shimizu 1992)

$$\frac{C_i^1}{C_i^o} = \frac{1}{D_i^o + (1-P_i)\alpha/(\alpha+1)} \left[\frac{(D_i^o+\alpha)-(P_i+\alpha)F}{(D_i^o+\alpha)-(P_i+\alpha)\alpha/(\alpha+1)}\right]^{((1-P_i)/(P_i+\alpha))}, \quad (2)$$

$C_i^1$ = Concentration of the element i in the liquid (*current liquid in the case of continuous melting*),

$C_i^o$ = Initial concentration of the element i in the original source,

$D_i^o$ = Initial solid bulk distribution coefficient $\sum X_i K_{d_i}$,

$P_i$= Weighted distribution coefficient of liquid,

$F$ = Degree of melting,

$\alpha$ = Amount of critical melt retained with the residue.

Source mineralogy and melting proportions (Gurenko and Chaussidon 1995)

| Phase proportions | Gt–Sp Lherzolite | Sp Lherzolite |
|---|---|---|
| Ol | 0.55 | 0.53 |
| Opx | 0.22 | 0.24 |
| Cpx | 0.15 | 0.20 |
| Sp | 0.02 | 0.03 |
| Gt | 0.06 | 0.00 |
| Melting proportions | | |
| Ol | –0.10 | –0.30 |
| Opx | 0.25 | 0.40 |
| Cpx | 0.61 | 0.82 |
| Sp | 0.04 | 0.08 |
| Gt | 0.20 | 0.00 |

Mineral/melt partition coefficients (McKenzie and O' Nions 1991; Shaw 2000)

| | Ol | Opx | Cpx | Sp | Gt |
|---|---|---|---|---|---|
| La | 0.000053 | 0.000044 | 0.0536 | 0.00002 | 0.01 |
| Ce | 0.000125 | 0.00014 | 0.0858 | 0.00003 | 0.021 |
| Pr | 0.000251 | 0.00033 | 0.137 | 0.0001 | 0.054 |
| Nd | 0.000398 | 0.00052 | 0.1873 | 0.0002 | 0.087 |
| Pm | | | | | |
| Sm | 0.00065 | 0.0016 | 0.291 | 0.0004 | 0.217 |
| Eu | 0.0008 | 0.0033 | 0.329 | 0.0006 | 0.32 |
| Gd | 0.0015 | 0.005 | 0.367 | 0.0009 | 0.498 |
| Tb | 0.0021 | 0.0067 | 0.405 | 0.0012 | 0.75 |
| Dy | 0.0027 | 0.0084 | 0.442 | 0.0015 | 1.06 |
| Ho | 0.005 | 0.0127 | 0.415 | 0.0023 | 1.53 |
| Er | 0.01 | 0.017 | 0.387 | 0.003 | 2 |
| Tm | 0.016 | 0.025 | 0.409 | 0.0038 | 3 |
| Yb | 0.027 | 0.033 | 0.43 | 0.0045 | 4.03 |
| Lu | 0.03 | 0.041 | 0.433 | 0.0053 | 5.5 |

## References


Appavadhanulu K, Setti DN, Badrinarayanan S, Subba Raju M (1976) The Chimalpahad meta-anorthosite complex, Khammam district, Andhra Pradesh. Geol Surv India Misc Publ 23, pp 267–278

Arndt NT, Kerr AC, Tarney J (1997a) Dynamic melting in plume heads: the formation of Gorgana komatiites and basalts. Earth Planet Sci Lett 146:289–301

Arndt NT, Albarede F, Nisbet EG (1997b) Mafic and ultramafic magmatism. In: de Wit MJ, Ashwal LD (eds) Greenstone belts. Oxford University Press, London, pp 233–254

Ashwal LD (1993) Anorthosites. Springer, Germany, pp 422

Babu VRRM (1998) The Nellore schist belt: an Archaean greenstone belt, Andhra Pradesh, India. Gondwana Res Gr Mem 4:97–136

Eggins SM (1992) Petrogenesis of Hawaiian tholeiites: 2, aspects of dynamic melt segregation. Contrib Mineral Petrol 110:398–410

Elliott TR, Hakesworth CJ, Gronvold K (1991) Dynamic melting of the Iceland plume. Nature 351:201–206

Elthon D (1984) Plagioclase buoyancy in oceanic basalts: chemical effects. Geochim Cosmochim Acta 48:753–768

Ford CE, Russel DG, Frisk MR (1983) Olivine–liquid equilibria: temperature, pressure and composition dependence of crystal/liquid partition coefficients for Mg, $Fe^{2+}$, Ca and Mn. J Petrol 24:256–265

Francis D, Ludden J, Johnstone R, Davis W (1999) Picrite evidence for more Fe in Archean mantle reservoirs. Earth Planet Sci Lett 167:197–213

Frey FA, Bryan WB, Thompson G (1974) Atlantic ocean floor: geochemistry and petrology of basalts from Legs 2 and 3 of the Deep Sea Drilling Project. J Geophys Res 79:5507–5527

Gurenko AA, Chaussidon M (1995) Enriched and depleted primitive melts in olivine from Icelandic tholeiites: origin by continuous melting of a single mantle column. Geochim Cosmochim Acta 59:2905–2917

Hanski EJ, Smolkin VF (1995) Iron- and LREE-enriched mantle source for early Proterozoic intraplate magmatism as exemplified by the Pechenga ferropicrites, Kola Peninsula, Russia. Lithos 34:107–126

Hanson GN (1980) Rare earth elements in petrogenetic studies of igneous systems. Annu Rev Earth Planet Sci 8:371–406

Hanson GN, Langmuir CH (1978) Modeling of major elements in mantle-melt systems using trace element approaches. Geochim Cosmochim Acta 42:725–741

Hari Prasad B, Okudaria T, Hayasaka Y, Yoshida M, Divi RS (2000) Petrology and geochemistry of amphibolites from the Nellore–Khammam schist belt, SE India. J Geol Soc India 56:67–78

Kay R, Hubbard NS, Gast PW (1970) Chemical characteristics and origin of oceanic ridge volcanic rocks. J Geophys Res 75:1585–1613

Kerrich R, Wyman D, Fan J, Bleeker W (1998) Boninite series: low Ti-tholeiite associations from the 2.7 Ga Abitibi greenstone belt. Earth Planet Sci Lett 164:303–316

Kinzler RJ, Grove TL (1992) Primary magmas of mid-ocean ridge basalts 1. Experiments and methods. J Geophys Res 97:6885–6906

Langmuir CH, Bender JF, Bence AE, Hanson GN, Taylor SR (1977) Petrogenesis of basalts from the FAMOUS area: Mid-Atlantic ridge. Earth Planet Sci Lett 36:133–156

Langmuir CH, Hanson GN (1980) An evaluation of major element heterogeneity in the mantle sources for basalts. Philos Trans R Soc Lond A 297:383–407

Leelanandam C, Narsimha Reddy MN (1985) Petrology of the Chimalpahad anorthosite complex, Andhra Pradesh, India. Neues Jahrbuch Miner Abh 153:91–119

Maaløe S (1994) Estimation of the degree of partial melting using concentration ratios. Geochim Cosmochim Acta 58:2519–2525

Masuda A, Nakamura N, Tanaka T (1973) Fine structures of mutually normalized rare-earth patterns of chondrites. Geochim Cosmochim Acta 37:239–248

McKenzie D, O'Nions RK (1991) Partial melt distributions from inversion of rare earth element concentrations. J Petrol 32:1021–1091

Naqvi SM, Rogers JSW (1987) Geology of India. Oxford Monographs in Geology and Geophysics No. 6, Oxford University Press, Oxford, 223 pp

Pearce JA, Cann JR (1973) Tectonic setting of basic volcanic rocks determined using trace element analyses. Earth Planet Sci Lett 19:290–300

Prinzhofer A, Allegre CJ (1985) Residual peridotites and mechanisms of partial melting. Earth Planet Sci Lett 74:251–265

Radhakrishna BP, Naqvi SM (1986) Precambrian crust of India and its evolution. J Geol 94:145–166

Rajamani V, Balakrishnan K, Hanson GN (1993) Komatiite genesis: insights provided by Fe–Mg exchange equilibria. J Geol 101:809–819

Rajamani V, Shirey SB, Hanson GN (1989) Fe-rich Archaean tholeiities derived from melt-enriched mantle sources: evidence from the Kolar schist belt, South India. J Geol 97:487–501

Rajamani V, Shivkumar K, Hanson GN, Shirey SB (1985) Geochemistry and petrogenesis of amphibolites, Kolar schist belt, South India: evidence for komatiitic magma derived by low percentage of melting of mantle. J Petrol 26:92–123

Ramakrishnan M (2003) Craton-mobile belt relations in southern granulite terrain. Mem Geol Soc India 50:1–24

Sarvothaman H (1995) Amphibolites of Khammam schist belt: evidence for the Precambrian Fe-tholeiitic volcanism in marginal zone. Indian Mineral 49:177–186

Satyanarayana K, Dhana Raju R, Kanungo DN (1994) Geochemistry of amphibolites from the Nellore schist belt, Andhra Pradesh, India: an example of Back-arc basin low-K tholeiitic magmatism. J Geol Soc India 44:253–265

Schilling J-G (1966) Rare earth fractionation in Hawaiian volcanic rocks. Unpublished Ph.D. thesis, Massachusetts Institute of Technology

Schilling J-G (1973) Iceland mantle plume. Nature 246:141–143

Shaw DM (2000) Continuous (dynamic) melting theory revisited. Can Mineral 38:1041–1063

Sheraton JW (1984) Chemical changes associated with high-grade metamorphism of mafic rocks in the east Antarctic shield. Chem Geol 47:135–157

Sobolev AV, Shimizu N (1992) Ultra-depleted melts and permeability of the oceanic mantle (in Russian). Doklady Acad Sci Russia 236:354–360

Sobolev AV, Shimizu N (1993) Ultra-depleted primary melt included in an olivine from the Mid-Atlantic Ridge. Nature 363:151–154

Strong DF, Dostal J (1980) Dynamic melting of Proterozoic upper mantle: evidence from rare earth elements in oceanic crust of Eastern Newfoundland. Contrib Mineral Petrol 72:165–173

Sun S-s, Nesbitt RW (1978) Petrogenesis of Archaean ultrabasic and basic volcanics: evidence from rare earth elements. Contrib Mineral Petrol 65:301–325

Takahashi E (1986) Melting of dry peridotite KLB1 up to 14 GPa: implications on the origin of peridotite upper mantle. J Geophys Res 91:9367–9382

Takahashi E, Kushiro I (1983) Melting of dry peridotite at high pressures and basalt magma genesis. Am Mineral 68:859–879

Thompson G (1991) Metamorphic and hydrothermal processes: basalt-seawater interactions. In: Floyd PA (ed) Oceanic basalts, Blackie, Glasgow, pp 148–173

Vasudevan D, Kroner A, Wendt I, Tobschall H (2003) Geochemistry, Petrogenesis and age of felsic to intermediate metavolcanic rocks from the Palaeoproterozoic Nellore schist belt, Vinjamur, Andhra Pradesh, India. J Asian Earth Sci, in press

Weaver BL, Tarney J (1981) Chemical changes during dyke metamorphism in high-grade basement terrains. Nature 289:47–49

Wood DA (1979) Dynamic partial melting: its application to the petrogenesis of basalts erupted in Iceland, the Faeroe Islands, the Isle of Skye (Scotland) and the Troodos Massif (Cyprus). Geochim Cosmochim Acta 43:1031–1046

Zindler A, Hart SR, Frey FA, Jakobsson SP (1979) Nd and Sr isotope ratios and rare element abundances in Reykjanes Peninsula basalts: evidence for mantle heterogeneity beneath Iceland. Earth Planet Sci Lett 45:249–262

Zou H, Zindler A (1996) Constraints on the degree of dynamic partial melting and source composition using concentration ratios in magmas. Geochim Cosmochim Acta 60:711–717